




Optimizing the design of broadband solar metamaterial absorbers based on titanium nitride nanorings [Invited]

DO T. NGA,^{1,9} ANH D. PHAN,^{2,3,10} VU D. LAM,⁴  TREVON BADLOE,⁵  AND JUNSUK RHO^{6,7,8} 

¹*Institute of Physics, Vietnam Academy of Science and Technology, 10 Dao Tan, Ba Dinh, Hanoi 12116, Vietnam*

²*Faculty of Materials Science and Engineering, Phenikaa University, Hanoi 12116, Vietnam*

³*Phenikaa Institute for Advanced Study, Phenikaa University, Hanoi 12116, Vietnam*

⁴*Graduate University of Science and Technology, Vietnam Academy of Science and Technology, 18 Hoang Quoc Viet, Hanoi, Vietnam*

⁵*Graduate School of Artificial Intelligence, Pohang University of Science and Technology (POSTECH), Pohang 37673, Republic of Korea*

⁶*Department of Mechanical Engineering, Pohang University of Science and Technology (POSTECH), Pohang 37673, Republic of Korea*

⁷*Department of Chemical Engineering, Pohang University of Science and Technology (POSTECH), Pohang 37673, Republic of Korea*

⁸*POSCO-POSTECH-RIST Convergence Research Center for Flat Optics and Metaphotonics, Pohang 37673, Republic of Korea*

⁹*dtnga@iop.vast.vn*

¹⁰*anh.phanduc@phenikaa-uni.edu.vn*

Abstract: We propose a design rule for broadband metamaterial absorbers and investigate their plasmonic properties under solar irradiation. The metamaterials consist of periodic arrays of titanium nitride (TiN) rings placed on an antireflective MgF₂ dielectric film on a TiN bottom layer. We simulate the absorption of our metamaterials and find the dependence of the optical spectrum on structural parameters. From this, we propose a simple rule to design the nanostructures with an average spectral absorptivity greater than 95% over the solar spectrum from 200 to 3000 nm. Particularly, we introduce, for the first time, metamaterial perfect absorbers that can be designed using two-layer structures instead of higher-layer structures as conventional and sandwich designs. Our study would pave the way for great potential applications in the fields of solar energy harvesters and photo-to-thermal converters.

© 2023 Optica Publishing Group under the terms of the [Optica Open Access Publishing Agreement](#)

1. Introduction

To overcome the energy crisis that is restricting economic and social development, renewable energy is the primary solution. Solar energy is one of the cleanest and most abundant energy resources, which has been intensively studied to resolve the energy crisis. To effectively utilize solar energy, it is crucial to create novel structures with ultra-high and broadband absorption of light in the ultraviolet to near-infrared range (0.2–3.0 μm) [1–4]. The absorbed solar energy can be efficiently converted into heat to warm up objects and surrounding medium via the photothermal mechanism or into electricity via the photoelectric mechanism [1–4]. A wide range of different applications can be designed using these two mechanisms.

Metamaterials are artificial materials composed of subwavelength structures of metallic and dielectric materials arranged periodically [5,6]. They exhibit extraordinary electromagnetic properties that cannot be found in nature [5,6]. Over the past few years, there has been extensive research on metamaterial perfect absorbers with high absorption rates over a wide

range of wavelengths [5,7–14]. The study of broadband metamaterial absorbers can lead to the development of efficient solar energy harvesters and photo-to-thermal converters to address the energy crisis. In general, noble metals like gold or silver have been widely exploited to fabricate metamaterials since plasmonic properties of these materials can enhance absorption by manipulating light-matter interactions [1–6,11]. However, the low melting point of noble metals limits their use in high-temperature applications [15–17].

Alternative plasmonic materials like transition metal nitrides (such as TiN) have recently been suggested to replace conventional materials [15–18]. TiN has several advantages including stable thermodynamic properties at high temperatures, simple fabrication, compatibility with standard silicon devices, and lower production costs [15–17]. Although titanium nitride has a similar optical spectrum to gold in the near-infrared and visible ranges, its real permittivity is smaller due to its lower carrier concentration. Furthermore, the optical properties of TiN can be easily adjusted by altering the processing conditions.

Scientists have proposed various types of ultra-high absorptivity solar absorbers based on TiN nanostructures. Liu [19], Mehrabi [20], Habil [21], and Zhong [22] designed ultra-broadband perfect solar absorbers based on stacked layers of TiN/TiO₂ metasurfaces on a two-layered substrate. Meanwhile, Wu [23] proposed arrays of TiN and Si₃N₄ laminated ring structure on a three-layer substrate. Although this configuration achieves more than 90% absorption in the range of 280–300 nm and geometrical parameters can be optimized to obtain near-unity light absorption, their nanostructures become complicated with multilayers (more than four layers) and have multiple structural factors to control the absorption. The complexity of metamaterial structures could lead to high manufacturing costs and limit their potential applications. In other works, some sandwiched three-layer structures formed by an array of TiN rings [24–26] or cylinders [27,28] or cones [29]/dielectric layer/aluminum or TiN substrate have been investigated to attain perfect light absorption. Although these designs are simpler, the metamaterials only have nearly good absorption in the visible-to-near infrared band.

In a very recent work, Sun and his coworkers [30] also studied the structure of TiN nano-ring array, silica (SiO₂) dielectric film, and TiN bottom layer and found that their metamaterials are perfect absorbers in the wavelength range from 300–2500 nm. They used the electric and magnetic field distributions to indicate that the plasmonic coupling leads to high absorption. Although structural sizes are tuned to understand how the variation affects the absorption spectrum, no specific guidelines are provided for creating ideal metamaterial absorbers. In addition, only a single configuration was found to attain an absorption rate of 95% for AM1.5 spectral radiation.

There are several questions not previously addressed: (i) can we propose a simple design rule to design many structures of broadband perfect absorbers? (ii) can the proposed broadband metamaterials become simpler? (iii) how does the plasmonic coupling modify optical absorption? In this study, we use the finite difference time domain (FDTD) method to resolve all questions mentioned above. A simple design rule is proposed to fabricate perfect solar absorbers. Based on the guidelines, we found many structures for ultra-broadband metamaterials that have an absorption rate greater than 92% in the whole spectral region.

2. Theoretical background

Our proposed broadband absorber has a metal–insulator–metal structure, as shown in Fig. 1, composed of a square lattice of ring-shaped TiN nanostructures on a magnesium fluoride (MgF₂) dielectric layer thin film grown on a perfectly-reflective TiN substrate. The system can be experimentally fabricated using techniques described in Ref. [25,26]. The nanoring absorber was proved to exhibit higher absorption than the nanodisk and nanohole absorbers [26]. Here, we fixed the thickness of the bottom layer at 100 nm to mimic experiments in Ref. [25,26]. The structure is built using structural parameters: (1) a lattice period $L = 430$ nm as proposed in Ref. [30], (2) the height of the ring h_1 , (3) the inner and outer diameters of the TiN ring

being d and D , respectively, and (4) the thickness of the MgF_2 layer h_2 . To obtain the perfect metamaterial absorbers, we find $D-d = 30 \text{ nm}$ and $h_1 = D$. Note that the penetration depth of TiN ($\delta = \lambda / (4\pi \text{Im}(\sqrt{\epsilon_{\text{TiN}}}))$) approximately varies from 8 to 25 nm across the solar spectrum. Here, λ and ϵ_{TiN} are the wavelength and dielectric function of TiN, respectively. Consequently, when the thickness of the TiN ring is set to be 15 nm, it facilitates plasmonic coupling between inner and outer surfaces of the rings. This design rule suggests the number of decisive structural parameters reduces to 2 (h_2 and D). We follow the structural design guidelines in our subsequent calculations.

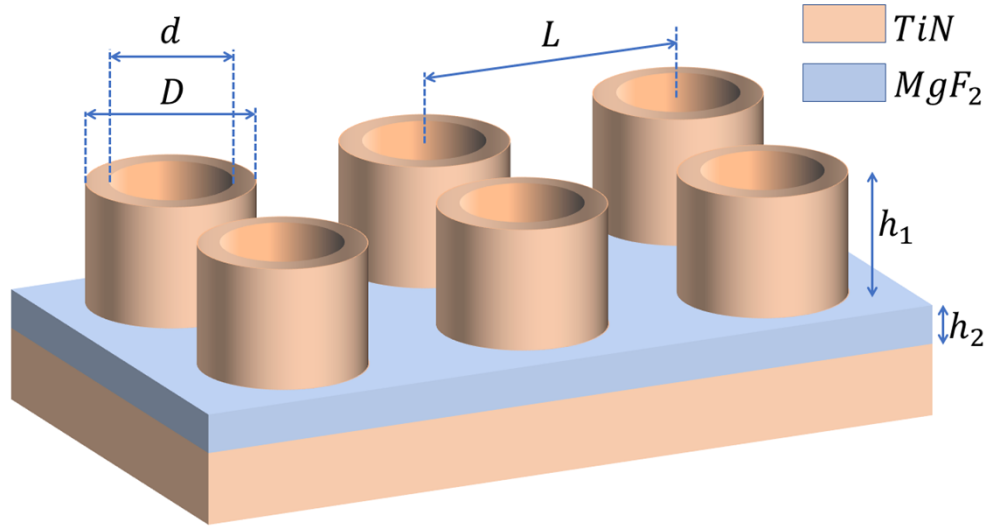


Fig. 1. The ultra-broadband metamaterial based on periodic arrays of TiN ring placed on dielectric thin films of MgF_2 , and a TiN substrate.

There are several reasons why MgF_2 is often preferred over SiO_2 as the dielectric spacer layer in certain applications. First, MgF_2 has a lower refractive index and this leads to less reflection and greater transmission of light through the structure [31,32]. Second, MgF_2 has a wider transmission range in the UV region compared to SiO_2 [31]. Third, the thermal conductivity of MgF_2 (11.6 W/m/K) is much higher than that of SiO_2 (1.38 W/m/K) [33]. Thus, MgF_2 is more suitable for high-temperature devices. In other applications, one can consider SiO_2 due to lower cost and higher chemical resistance.

We use FDTD solver in Computer Simulation Technology (CST) microwave studio software [34] to compute the absorption spectrum of the proposed metamaterial. The incident electromagnetic wave is a plane wave perpendicular to the surface. Its electric and magnetic components are parallel to the y-axis and x-axis, respectively. The open boundary condition is applied along the z-axis. Meanwhile, we employ the periodic boundary conditions along the x and y axes. The structure is excited using the Folquet port. The transmitter and receiver are positioned on opposite sides of the structure along the z-axis to determine the reflection and transmission coefficient. Then, the absorption A of broadband metamaterial absorbers is calculated by $A = 1 - R - T$, where R and T are the reflectance and transmittance, respectively. The dielectric function of TiN and MgF_2 are taken from Ref. [35] and [36], respectively. The dielectric function is a complex permittivity, which consists of a real part (ϵ') and an imaginary part (ϵ''). Figure 2 shows experimental data of the dielectric function of TiN and MgF_2 as a function of wavelength [35,36]. The usage provides more accurate results than fixing the dielectric function of MgF_2 to be constant.

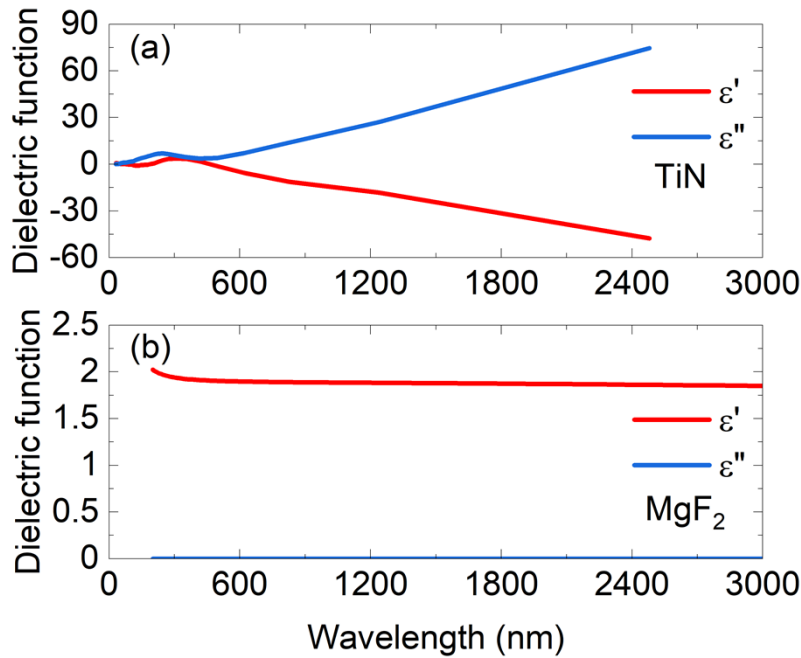


Fig. 2. The real (ϵ') and imaginary (ϵ'') part of the dielectric function for (a) TiN and (b) MgF_2 over wavelengths from 200 nm to 3000 nm.

To evaluate the effectiveness of our broadband metamaterials in collecting solar energy, we compute the average spectral absorptivity of the absorbers as

$$\alpha_{solar} = \frac{\int_{\lambda_{min}}^{\lambda_{max}} A(\lambda) E_{\lambda} d\lambda}{\int_{\lambda_{min}}^{\lambda_{max}} E_{\lambda} d\lambda} \quad (1)$$

where E_{λ} is the AM1.5 global solar spectrum, λ_{min} and λ_{max} are 200 nm and 3000 nm, respectively. The total solar absorptance can be understood as the percentage of absorbed energy in the AM1.5 spectral radiation.

3. Results and discussions

Our calculations begin with the simplest structure which we assume $h_2 = 0$. The three-layer sandwich structure becomes a two-layer system. Figure 3(a) shows the spectral absorbance of the absorber in the 200-3000 nm range as varying the outer diameter of the TiN ring. The wavelength range in our calculations is beyond the range of experimental dielectric data of TiN ($\lambda \leq 2480$ nm) in Fig. 2, the validity of our absorption predictions within the wavelength range of 2480-3000 nm was confirmed in the Supplementary Materials. Remarkably, one can observe excellent broadband absorption in this solar spectral range. When the outer diameter of TiN rings is small ($D \leq L/2$), the plasmonic coupling among nanostructures is neglectable and, thus, the optical absorption of the metamaterials is not high. Increasing D from 240 nm to 340 nm significantly enhances the plasmonic coupling and harvests more sunlight in the solar spectral region. Numerical results in Fig. 3(b) clearly indicate that the mean spectral absorptivity grows from 88% to 95.2%. This suggests, for the first time, that it is possible to create perfect metamaterial absorbers using two-layered periodic plasmonic structures without a dielectric layer. As the size of TiN rings is increased further, the impact of the scattering process on the interaction

between light and matter becomes more prominent, leading to a decrease in absorption. As a result, the mean absorption rate experiences a slight reduction from 95.2% to 92.2% with an increase in D from 340 nm to 400 nm.

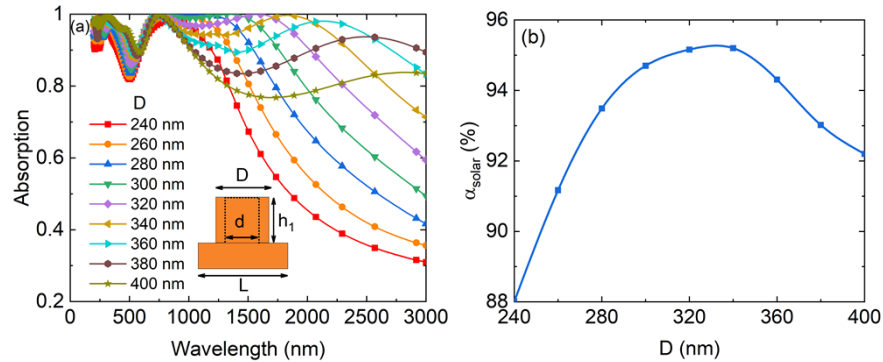


Fig. 3. (a) Absorption spectra for systems having $h_2 = 0$ at different outer diameters of TiN rings. (b) The average spectral absorptivity as a function of the outer diameter of TiN rings in the range of 240-400 nm.

The absorption mechanism in the TiN-based metamaterials originates from the interplay between localized surface plasmon resonance and the inherent loss of TiN. The real part of the dielectric function represents how a material responds to electric fields, while the imaginary part accounts for energy absorption and dissipation. When the real part of the dielectric function of TiN (ϵ') is positive, as in the case of dielectric materials, the collective oscillation of electrons is dampened, and the localized surface plasmon resonance (LSPR) is less likely to occur. The incident light is slightly absorbed by the TiN nanoring layer. Thus, the contribution of the intrinsic loss of TiN (particularly, the bottom flat layer) to the absorption plays an important role. Meanwhile, when ϵ' is negative as is the case for many metals ($\lambda \geq 462$ nm), the free electrons of TiN can collectively oscillate in response to the incident electric field, giving rise to LSPR. TiN has metallic properties and becomes an alternative plasmonic material. An increase in wavelength induces larger values of ϵ'' and stronger light absorption. The electric field inside the TiN ring can be significantly enhanced due to cavity resonance. Meanwhile, the electric field is also tightly confined among the nanorings because of mutual interactions between the localized plasmonic resonances of neighboring nanostructures. The small thickness of the ring structure facilitates the interaction between the surface plasmons produced by the inner and outer TiN nanorings. As a result, the incident light is mainly absorbed by the nanoarray.

To have better understanding of physical mechanisms underlying the broadband perfect absorption of our metamaterials, we analyze the spatial distribution of electric and magnetic fields at $\lambda = 733$ and 1840 nm, which are two resonance peaks of the two-layer systems having $D = h_1 = 340$ nm, across a unit cell in Fig. 4. At a wavelength of 1840 nm, the distribution of the electric field exhibits an electric dipole resonance within the upper ring antenna, whereas the magnetic field distribution does not appear significant. The magnetic field is largely absorbed by both the TiN flat layer and rings. Furthermore, the electric and magnetic field is strongly enhanced outside the TiN rings. This finding clearly indicates that the absorption is predominantly influenced by the plasmonic coupling among the TiN rings. Interestingly, at $\lambda = 733$ nm, this plasmonic coupling remains to intensify the electric field within the gaps between nanostructures but the cavity resonance also leads to a significant enhancement of the electric field inside the TiN rings. Thus, the high absorption performance is attributed to the strong cavity resonance and plasmonic interactions among plasmonic nanorings.

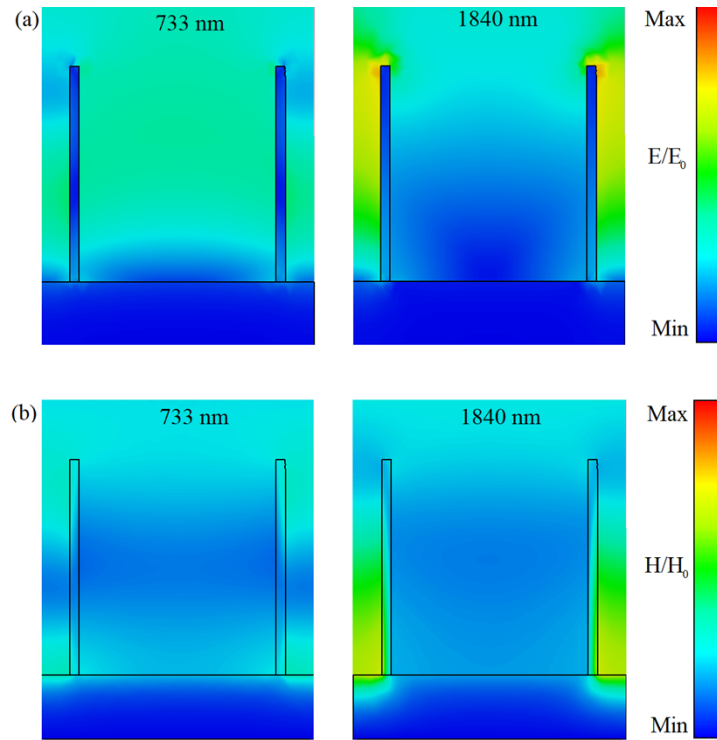


Fig. 4. (a) Electric and (b) magnetic field distribution at 733 and 1840nm in xz -plane for $y = 0$ nm.

Afterward, we conduct simulations to investigate how the thickness of the MgF_2 spacer layer affects the absorption of the TiN-based metamaterials. Figure 5 shows the computed absorption spectra of our proposed absorbers for various h_2 values. The metamaterials without the dielectric layer ($h_2 = 0$) exhibit good light absorption in the visible region. However, in the longer wavelength region, the metamaterials have relatively low absorption. The presence of the MgF_2 dielectric layer in the middle of two TiN layers can modify the resonances of the metamaterial structure and control over absorption peaks and bandwidth. This dielectric layer amplifies the electric field within the structure, enhances the interaction with incident electromagnetic waves, and thus increases the absorption performance. In addition, the dielectric layer can serve as an impedance-matching medium between the metamaterial and the surrounding environment. From this, the reflection can be minimized, and the absorption can be maximized. If these effects are compensated and mutually reinforcing, the absorption can be enhanced or remain unchanged. Numerical results in the mainframe of Fig. 5(a) reveal that the sandwiched three-layer structures with $D = h_1 = 240$ nm significantly enhance the absorption in the near-infrared region as increasing the dielectric thickness. Particularly, the maximum absorption reaches 100% in the range of 800 nm to 1500 nm when $h_2 \geq 60$ nm. Because of the opposite absorption trends in two different light regimes, one can expect a non-monotonic variation of the average spectral absorption as the dielectric spacer layer thickness increases. Numerical results in the inset of Fig. 5(a) clearly confirm this analysis. For $60 \text{ nm} \geq h_2 \geq 30 \text{ nm}$, $\alpha_{\text{solar}} \approx 93\%$ and it suggests that our design rule allows us to find many structures having the same absorption and we can choose the best design for mass production.

To study how the MgF_2 layer affects the optical absorption of the metamaterials having $D = h_1 = 340$ nm, we carry out simulations and show results in Fig. 5(b). In the wavelength range

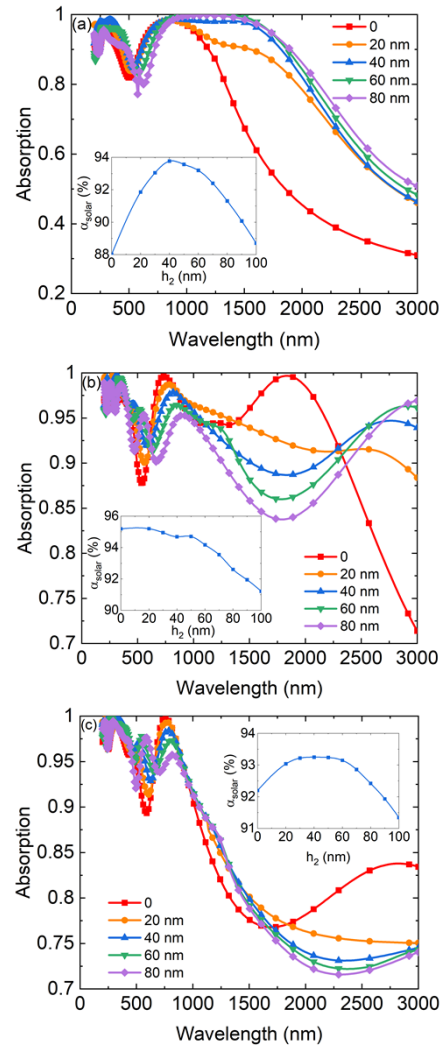


Fig. 5. Absorption spectra for systems having (a) $D = h_1 = 240$ nm, (b) $D = h_1 = 340$ nm, and (c) $D = h_1 = 400$ nm at different thicknesses of the MgF₂ layer. The inset shows the average spectral absorptivity as a function of the thickness of the MgF₂ layer.

from 200 nm to 2300 nm, the absorption band is lowered when the dielectric layer becomes thicker. Although the variation of the absorption band at higher wavelengths is reversed, the optical energy in this range is extremely small. Simulation results in the inset of Fig. 5(b) indicate that $h_2 = 0$ is an optimal structure parameter for our proposed broadband metamaterials. α_{solar} monotonically decreases with increasing h_2 . Adding the MgF₂ layer slightly modifies the absorption as $h_2 \leq 30$ nm and moderately decreases the light energy harvesting efficiency as $h_2 > 30$ nm. Consequently, the two-layered metamaterial is not only the simplest structure but also the strongest absorption over the spectral range.

We compute the absorption spectra for metamaterials having $D = h_1 = 400$ nm at different values of h_2 and show results in Fig. 5(c). When the wavelength is less than 1600 nm, the absorption spectrum remains nearly unchanged with varying thicknesses of the MgF₂ layer. The percentage of absorbed energy in the solar region (0.2–3 μm) fluctuates non-linearly from 91.3%

to 93.25% for dielectric layer thicknesses less than 100 nm as shown in the inset of Fig. 5(c). Thus, it is possible to design ultrawideband solar energy absorbers performing similar photon-to-heat conversion efficiency.

Altering the distance between the inner and outer surface of TiN rings has a significant impact on optical absorption. To study how the thickness of the ring affects the energy harvesting systems, we perform simulations by setting $D = h_1 = 340$ nm and $h_2 = 0$ and changing the inner radius of TiN rings. The predicted spectral evolution is shown in Fig. 6(a). An increase in TiN ring thickness enhances optical absorption over the UV and visible range of 200 to 800 nm but weakens absorption bands in the near-infrared range. Thus, the average absorption rate in the spectral range exhibits a non-trivial change as the thickness of the TiN rings varies (seen in Fig. 6(b)). The maximum percentage of absorbed energy occurs when $D-d = 30$ nm. This result confirms that $D-d = 30$ nm is the optimal geometric parameter in our proposed design. At this size, the ring structure is sufficiently thin to enable the surface plasmon on the inner and outer surfaces of the ring to maximally couple with each other. However, increasing the thickness of the ring reduces the coupling between the electric field inside and outside the ring, and also leads to a decrease in the percentage of absorbed energy.

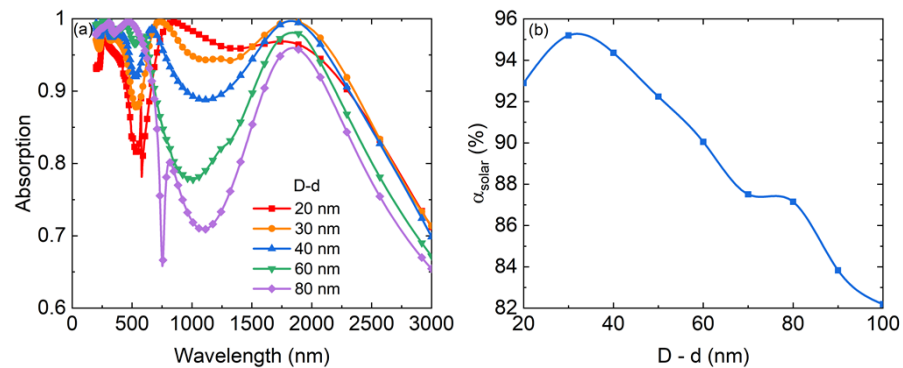


Fig. 6. (a) Absorption spectra for systems having $h_2 = 0$ and $D = h_1 = 340$ nm at different TiN-ring thicknesses. (b) The total solar absorptance as a function of the thickness of TiN rings in the range of 20-100 nm.

It is known that the incident angle has a strong effect on the absorption of structures [19,22,25,28]. In Fig. 7, we calculate the absorption spectrum of the two-layer metamaterials having $D = h_1 = 340$ nm at different incident angles from 0° to 80° . The incident angle is determined by the angle at which the incident wave vector intersects with the surface normal of the metamaterials. In the LSPR region ($\lambda \geq 462$ nm), an increase in the incident angle leads to a decrease in absorption. There are several reasons to explain the optical variation. First, at normal incidence, the incident light is perpendicular to the surface, the electromagnetic field penetrates the metamaterial more effectively and interacts with a large area of the TiN rings. This maximizes the chance of light absorption. As the incident angle increases, the effective area of interaction between the incident light and the TiN rings decreases. Second, at a shallower angle, the light travels through a longer path of the material. The elongated path means that the light has more opportunities to scatter, reflect, and transmit rather than being absorbed. Third, the orientation of the electric field changes. Thus, the efficiency of coupling with the resonant modes of the metamaterial is reduced and the interaction between the light and the TiN rings is weakened. Fourth, the resonance conditions can be shifted. The mismatch between the incident light's frequency and the metamaterial's resonance frequency can decrease absorption efficiency.

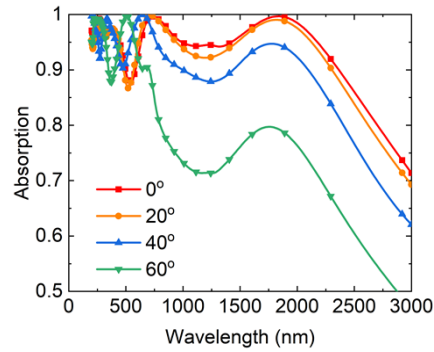


Fig. 7. Absorption spectra for systems having $h_2 = 0$ and $D = h_1 = 340$ nm at different incident angles.

To compare the structural design and absorption efficiency of our proposed metamaterials with previous studies, we calculate the average absorption by

$$\alpha_{ave} = \frac{\int_{\lambda_{min}}^{\lambda_{max}} A(\lambda) d\lambda}{\lambda_{max} - \lambda_{min}} \quad (2)$$

and summarize structural designs, materials, operating bands, and their absorption efficiency in Table 1. It clearly shows that our structure is much simpler, while the largest average absorption rate over a wide range of wavelengths is high. Other designs for broadband metamaterial absorbers can have higher absorption but the structures are complicated and, thus, it is more difficult to mass production.

Table 1. TiN-based broadband metamaterial absorbers with different designs and their absorption performance

Design	Materials	Number of layers	Operating band (nm)	Average absorption (%)
Ti/TiN multilayer ring structure [23]	Si ₃ N ₄ /TiN/Ti	6	280-3000	98
TiN-nanocone metasurface [29]	TiN/Al ₂ O ₃	3	400-1500	≥ 96
TiN nanodisk and four symmetrically wrapped nanotriangles [28]	TiN/MgF ₂	3	350-800	98.3
Hexagonal TiN nanodisk array [27]	TiN/SiO ₂ /Al	3	400-850	98.1
TiO/TiN half-cylinder nanograting [22]	TiN/TiO ₂	4	380-760	94
TiO ₂ /TiN composite nanodisks [19]	TiN/TiO ₂ /SiO ₂	4	316-1426	> 90
TiN/TiO ₂ stacked square-layers [20]	TiN/TiO ₂	7	200-2800	96
Truncated cone-shaped TiO ₂ core surrounded by conical TiO ₂ /TiN rings [21]	TiN/TiO ₂ /Si	7	200-3250	99
TiN nanorings [25,26]	TiN/SiO ₂	3	400-900	≥ 95
TiN nanorings [30]	TiN/SiO ₂	3	300-2500	97.6
This study	TiN	2-3	200-3000	93.6

4. Conclusion

We have proposed a design rule for perfect metamaterial absorbers operating over the spectral region from 200 nm to 3000 nm. The structure consists of three layers including a TiN bottom film, a MgF₂ dielectric film, and a square lattice of TiN nanorings. Our designs are based on three rules including the ring thickness equal to 15 nm, the height of TiN rings equal to the outer diameter of TiN rings, and the outer diameter of TiN rings larger than half of a lattice period to have plasmonic coupling. The proposed solar absorber shows promising energy absorption capability in the AM1.5 radiation spectrum with a ratio of 95.2%. Many structures can be found to have a solar absorption rate larger than 92%. Remarkably, a novel absorber structure based on two-TiN layers provides the best optical absorption. The dielectric layer is for designing ultra-wide perfect absorbers. Similar impedance matching conditions have also been employed for perfect transmission using metasurfaces [37]. Previous absorbers have been fabricated using standard electron-beam lithography techniques, with some examples of direct laser inscription [38]. These approaches could also be used to experimentally realize the absorbers demonstrated here, while shadow sphere lithography is another potential method of fabricating such ring structures of TiN [26]. The findings of this research would pave the way for the advancement and utilization of solar collectors and thermophotovoltaics.

Funding. POSCO (POSCO-POSTECH-RIST Convergence Research Center); Vietnam Academy of Science and Technology (KHCBVL.05/22-23); Institute for Information and Communications Technology Promotion (2019-0-01906); National Research Foundation of Korea (NRF-2022M3C1A3081312).

Acknowledgments. This research is funded by Vietnam Academy of Science and Technology under grant number KHCBVL.05/22-23. J.R. acknowledges the POSCO-POSTECH-RIST Convergence Research Center program funded by POSCO, and the National Research Foundation (NRF) grant (NRF-2022M3C1A3081312) funded by the Ministry of Science and ICT (MSIT) of the Korean government. T.B. acknowledges the Institute of Information & Communications Technology Planning & Evaluation (IITP) grant (No. 2019-0-01906, the POSTECH Artificial Intelligence Graduate School program) funded by the MSIT of the Korean government, and the POSTECH PIURI fellowship.

Disclosures. The authors declare no conflicts of interest.

Data availability. Data underlying the results presented in this paper are not publicly available at this time but may be obtained from the authors upon reasonable request.

Supplemental document. See [Supplement 1](#) for supporting content.

References

1. P. Cheng, D. Wang, and P. Schaaf, "A Review on Photothermal Conversion of Solar Energy with Nanomaterials and Nanostructures: From Fundamentals to Applications," *Adv. Sustainable Syst.* **6**(9), 2200115 (2022).
2. P. K. Nayak, S. Mahesh, H. J. Snaith, and D. Cahen, "Photovoltaic solar cell technologies: analysing the state of the art," *Nat. Rev. Mater.* **4**(4), 269–285 (2019).
3. M. Gao, L. Zhu, C. K. Peh, and G. W. Ho, "Solar absorber material and system designs for photothermal water vaporization towards clean water and energy production," *Energy Environ. Sci.* **12**(3), 841–864 (2019).
4. C. Chen, Y. Kuang, and L. Hu, "Challenges and Opportunities for Solar Evaporation," *Joule* **3**(3), 683–718 (2019).
5. B.-X. Wang, C. Xu, G. Duan, W. Xu, and F. Pi, "Review of Broadband Metamaterial Absorbers: From Principles, Design Strategies, and Tunable Properties to Functional Applications," *Adv. Funct. Mater.* **33**(14), 2213818 (2023).
6. J. E. Holliman Jr, H. T. Schaeff, B. P. McGrail, and Q. R. S. Miller, "Review of foundational concepts and emerging directions in metamaterial research: design, phenomena, and applications," *Mater. Adv.* **3**(23), 8390–8406 (2022).
7. M. A. Abbas, J. Kim, A. S. Rana, I. Kim, B. Rehman, Z. Ahmad, Y. Massoud, J. Seong, T. Badloe, K. Park, M. Q. Mehmood, M. Zubair, and J. Rho, "Nanostructured chromium-based broadband absorbers and emitters to realize thermally stable solar thermophotovoltaic systems," *Nanoscale* **14**(17), 6425–6436 (2022).
8. I. Sajedian, T. Badloe, H. Lee, and J. Rho, "Deep Q-network to produce polarization-independent perfect solar absorbers: a statistical report," *Nano Converg.* **7**(1), 26 (2020).
9. D. M. Nguyen, D. Lee, and J. Rho, "Control of light absorbance using plasmonic grating based perfect absorber at visible and near-infrared wavelengths," *Sci. Rep.* **7**(1), 2611 (2017).
10. A. S. Rana, M. Q. Mehmood, H. Jeong, I. Kim, and J. Rho, "Tungsten-based Ultrathin Absorber for Visible Regime," *Sci. Rep.* **8**(1), 2443 (2018).
11. H. Hajian, A. Ghobadi, B. Butun, and E. Ozbay, "Active metamaterial nearly perfect light absorbers: a review [Invited]," *J. Opt. Soc. Am. B* **36**(8), F131–F143 (2019).
12. N. I. Landy, S. Sajuyigbe, J. J. Mock, D. R. Smith, and W. J. Padilla, "Perfect Metamaterial Absorber," *Phys. Rev. Lett.* **100**(20), 207402 (2008).

13. K. Aydin, V. E. Ferry, R. M. Briggs, and H. A. Atwater, "Broadband polarization-independent resonant light absorption using ultrathin plasmonic super absorbers," *Nat. Commun.* **2**(1), 517 (2011).
14. A. Tittl, M. G. Harats, R. Walter, X. Yin, M. Schaferling, N. Liu, R. Rapaport, and H. Giessen, "Quantitative angle-resolved small-spot reflectance measurements on plasmonic perfect absorbers: impedance matching and disorder effects," *ACS Nano* **8**(10), 10885–10892 (2014).
15. P. R. West, S. Ishii, G. V. Naik, N. K. Emani, V. M. Shalaev, and A. Boltasseva, "Searching for better plasmonic materials," *Laser Photonics Rev.* **4**(6), 795–808 (2010).
16. G. V. Naik, V. M. Shalaev, and A. Boltasseva, "Alternative Plasmonic Materials: Beyond Gold and Silver," *Adv. Mater.* **25**(24), 3264–3294 (2013).
17. Y. Gutierrez, A. Brown, F. Moreno, and M. Losurdo, "Plasmonics beyond noble metals: Exploiting phase and compositional changes for manipulating plasmonic performance," *J. Appl. Phys.* **128**(8), 080901 (2020).
18. M. Dasog, "Transition Metal Nitrides Are Heating Up the Field of Plasmonics," *Chem. Mater.* **34**(10), 4249–4258 (2022).
19. Z. Liu, G. Liu, Z. Huang, X. Liu, and G. Fu, "Ultra-broadband perfect solar absorber by an ultra-thin refractory titanium nitride meta-surface, Solar Energy Materials and Solar Cells," *Sol. Energy Mater. Sol. Cells* **179**, 346–352 (2018).
20. S. Mehrabi, R. Muhammad, H. Bilal, M. A. Naveed, and M. M. Ali, "Ultra-broadband nanostructured metamaterial absorber based on stacked square-layers of TiN/TiO₂," *Opt. Mater. Express* **12**(6), 2199–2211 (2022).
21. M. K. Habil, M. Ghahremani, and C. J. Zapata-Rodriguez, "Multi-octave metasurface-based refractory superabsorber enhanced by a tapered unit-cell structure," *Sci. Rep.* **12**(1), 17066 (2022).
22. H. Zhong, Z. Liu, P. Tang, X. Liu, X. Zhan, P. Pan, and C. Tang, "Thermal-stability resonators for visible light full-spectrum perfect absorbers," *Sol. Energy* **208**, 445–450 (2020).
23. P. Wu, S. Dai, X. Zeng, N. Su, L. Cui, and H. Yang, "Design of ultra-high absorptivity solar absorber based on Ti and TiN multilayer ring structure," *Int. J. Therm. Sci.* **183**, 107890 (2023).
24. I. Kim, S. So, A. S. Rana, M. Q. Mehmood, and J. Rho, "Thermally robust ring-shaped chromium perfect absorber of visible light," *Nanophotonics* **7**(11), 1827–1833 (2018).
25. D. Lee, M. Go, M. Kim, J. Jang, C. Choi, J. K. Kim, and J. Rho, "Multiple-patterning colloidal lithography-implemented scalable manufacturing of heat-tolerant titanium nitride broadband absorbers in the visible to near-infrared," *Microsyst. Nanoeng.* **7**(1), 14 (2021).
26. M. Go, D. Lee, S. Kim, J. Jang, K.-W. Kim, J. Lee, S. Shim, J. K. Kim, and J. Rho, "Facile Fabrication of Titanium Nitride Nanoring Broad-Band Absorbers in the Visible to Near-Infrared by Shadow Sphere Lithography," *ACS Appl. Mater. Interfaces* **15**(2), 3266–3273 (2023).
27. D. Huo, J. Zhang, H. Wang, X. Ren, C. Wang, H. Su, and H. Zhao, "Broadband Perfect Absorber with Monolayer MoS₂ and Hexagonal Titanium Nitride Nano-disk Array," *Nanoscale Res. Lett.* **12**(1), 465 (2017).
28. R.-Q. Piao, Q. Xu, W.-H. Wong, E. Y.-B. Pun, and D.-L. Zhang, "Metasurface Absorber: A Theoretical Study of Broadband Nearly Perfect Metasurface Absorber Based on Nanoarray of Titanium Nitride," *Adv. Theory Simul.* **2**(7), 1900042 (2019).
29. D. Huo, J. Zhang, Y. Wang, C. Wang, H. Su, and H. Zhao, "Broadband Perfect Absorber Based on TiN-Nanocone Metasurface," *Nanomaterials* **8**(7), 485 (2018).
30. C. Sun, H. Liu, B. Yang, K. Zhang, B. Zhang, and X. Wu, "An ultra-broadband and wide-angle absorber based on a TiN metamaterial for solar harvesting," *Phys. Chem. Chem. Phys.* **25**(1), 806–812 (2023).
31. T. Pilvi, T. Hatanpaa, E. Puukilainen, K. Arstila, M. Bischoff, U. Kaiser, N. Kaiser, M. Leskela, and M. Ritalaa, "Study of a novel ALD process for depositing MgF₂ thin films," *J. Mater. Chem.* **17**(48), 5077–5083 (2007).
32. E. Kemnitz, S. Mahn, and T. Krahl, "Nano metal fluorides: small particles with great properties," *ChemTexts* **6**(3), 19 (2020).
33. Corning Incorporated, "Advanced Optics," <https://www.corning.com/advanced-optics>.
34. The software of CST Microwave Studio, <http://www.cst.com/>.
35. J. Pfluger, J. Fink, W. Weber, K. P. Bohnen, and G. Crecelius, "Dielectric properties of TiC_x, TiN_x, VC_x, and VN_x from 1.5 to 40 eV determined by electron-energy-loss spectroscopy," *Phys. Rev. B* **30**(3), 1155–1163 (1984).
36. M. J. Dodge, "Refractive properties of magnesium fluoride," *Appl. Opt.* **23**(12), 1980–1985 (1984).
37. J. W. Lee, M. A. Seo, J. Y. Sohn, Y. H. Ahn, D. S. Kim, S. C. Jeoung, C. Lienau, and Q.-H. Park, "Invisible plasmonic meta-materials through impedance matching to vacuum," *Opt. Express* **13**(26), 10681–10687 (2005).
38. M. L. Tseng, Y.-W. Huang, M.-K. Hsiao, H. W. Huang, H. M. Chen, Y. L. Chen, C. H. Chu, N.-N. Chu, Y. J. He, C. M. Chang, W. C. Lin, D.-W. Huang, H.-P. Chiang, R.-S. Liu, G. Sun, and D. P. Tsai, "Fast Fabrication of a Ag Nanostructure Substrate Using the Femtosecond Laser for Broad-Band and Tunable Plasmonic Enhancement," *ACS Nano* **6**(6), 5190–5197 (2012).